Disclaimer

This note has not been internally reviewed by the DØ Collaboration. Results or plots contained in this note were only intended for internal documentation by the authors of the note and they are not approved as scientific results by either the authors or the DØ Collaboration. All approved scientific results of the DØ Collaboration have been published as internally reviewed Conference Notes or in peer reviewed journals.

LBL-23519

D0-#562

Test Results from a Precision Drift Chamber Vertex Detector Prototype Using Dimethyl Ether

A. R. Clark, F. Goozen, L. T. Kerth, C. Klopfenstein,

S. C. Loken, M. Strovink, and T. G. Trippe

Lawrence Berkeley Laboratory and Department of Physics,

University of California, Berkeley CA 94720

Results of beam tests of a prototype drift chamber vertex detector developed for the D-Zero experiment at the Fermilab collider are reported. The chamber design emphasizes dual goals of high accuracy position measurement and excellent two track resolution. These requirements are met by using a slow gas, dimethyl ether, in a jet chamber geometry with a double plane of field-shaping wires near the anodes. Resolution of nearby hits is facilitated by 100 MHz flash digitization of the signal pulses. The prototype tested consisted of a full-length (97 cm) model of one azimuthal sector of the innermost layer of the detector, with 8 anode wires. Position measurement accuracy of 30 − 80 μm for drift distances of 2 − 11 mm and pulse pair resolution of 0.7 mm (for 90% of all pulses) is achieved.

Submitted to Nuclear Instruments and Methods A.

I. Introduction

Recently several groups have investigated the use in drift chambers of non-saturated gases, *i.e.* gases for which the drift velocity is nearly proportional to the electric field [1,2,3,4]. The advantages of these gases are twofold. First, some non-saturated gases have much lower drift velocities (for practical E/p values) than commonly used saturated gases. Second, diffusion constants in non-saturated gases can be much smaller than in saturated gases, because of the lower mean energy of the drifting electrons. For these reasons non-saturated gases are often referred to as 'slow' or 'cool' gases. A particularly promising gas is dimethyl ether (DME). The drift velocity of electrons in DME is ≈ 3.3 μm/nsec at E/p = 1 kV/cm-atm, more than a factor 10 slower than P-10, for example. Diffusion in DME is very low, < 100 μm transverse to a 1 cm drift for E/p between 1 and 2 kV/cm-atm [1]. Position accuracy of better than 30 μm (at atmospheric pressure) has been measured in small chambers with somewhat idealized geometries [1,2]. In addition, existing evidence indicates that DME, if sufficiently pure, resists radiation damage relatively well [5].

We are constructing a drift chamber vertex detector that is designed for use with DME as well as other gases, as part of the D-Zero experiment at the Fermilab $\bar{p}p$ collider. The D-Zero detector is a large solid angle, non-magnetic detector for general purpose experimentation at the collider. The overall design emphasizes excellent calorimetry and electron and muon identification, for optimal measurement of leptons, jets and missing energy. In the central region the tracking system, shown in Fig. 1, consists of this drift chamber vertex detector, followed by a transition radiation detector (TRD) for electron identification and by an outer drift chamber. In addition to its use in conjunction with the outer drift chamber, the vertex detector serves as an independent track detector. In particular, it must find the charged tracks left by electrons before entering the TRD, in order to distinguish them from photons converting in the radiator material. The vertex detector also must have low enough radiation thickness not to generate excessive e^+e^- pair background through photon conversions. Finally, to the extent possible in this crowded

environment, it is also desirable to use this inner drift chamber to identify secondary vertices.

These multiple demands on the detector impose stringent requirements on its performance, while limiting the range of possible solutions. Choosing a slow gas is attractive for several reasons. First, a low electron drift velocity reduces the drift distance corresponding to the width of each time bucket for which chamber signals are flash digitized (10 nsec here). Then the digitizing frequency no longer limits either the single-hit accuracy or the two-hit resolution. Both the accuracy and resolution benefit further from sharper pulses due to the low diffusion and the high ratio of ion to electron mobility in a slow gas. To achieve comparably low diffusion in a fast gas, several atmospheres of pressure would be required, thickening the chamber ends unacceptably.

II. Chamber Geometry and Electrostatic Properties

We have chosen a jet chamber geometry for the vertex detector, rather than a hexagonal or cylindrical ("straw") layout. The primary reason is to obtain a large number of samples along a track while holding the electronics channel and cable count within reasonable limits. Also, the jet geometry is well suited to achieving good track-pair resolution in a gas with non-saturated drift velocity, since the electric field can be made uniform through most of the active volume.

In a jet chamber, optimizing the single-hit accuracy and two-hit resolution depends strongly on minimizing the time spread over which the ionization electrons arrive. This spread is affected by variations in the length of the electron drift path and in the electric field encountered along it, and also by stochastic effects (distribution of ionization clusters and diffusion). The non-stochastic effects are readily calculated for an ideal geometry consisting of a plane of anode ("sense") wires, one or two nearby planes of field-shaping ("grid") wires, and two parallel cathode planes far away (Fig. 2 inset). In addition to the electron mobility, the relevant variables are the ratio of the separation g between grid

planes to the spacing s between sense wires, and the ratio of the total charge Q(grid) on both grid planes to the charge Q(sense) on the sense plane. Figure 2 plots the time interval Δt required to collect 90% of the electrons created by a parallel track, expressed in units of s divided by the drift velocity in the constant-field region, vs. Q(grid)/Q(sense) for four different gases. The curves are labelled by the parameter g/s.

An immediate conclusion is that the non-stochastic time spread, expressed in these units, is about a factor 2 worse for an idealized slow gas (constant mobility, Fig. 2a) than for a gas with saturated drift velocity (Fig. 2b). In fact, for a drift velocity varying *inversely* with the electric field, the spread would vanish. This explains the unusually isochronous behavior achieved with A-CH_4-CO_2 and A-CH_4 mixtures when the constant field is chosen to lie just above the value corresponding to the Ramsauer peak in the drift velocity (Figs. 2c and 2d).

To benefit from using a slow gas, it is important to minimize this large time spread. Figure 2 shows the advantage of using two separate grid planes, as opposed to one. For a slow gas, the effect is most pronounced when $Q(\text{grid}) \approx -0.5\,Q(\text{sense})$. Then, as g increases, the field lines curve more gently in their transition from the constant-field volume to the region near the sense wires, improving the uniformity in electron arrival time.

Two effects limit the grid plane separation. Obviously one wants the region of uniform electric field, outside of the grid planes, to extend over most of the cell. By itself this is an important limit on g. A less obvious constraint is the effect of g on the electrostatic stability of the wires. This is especially important at the Fermilab collider, where the luminous region is 28 cm rms in length, and the unsupported wire span in this chamber ranges up to 115 cm. There are two important modes of coherent electrostatic instability. The "out of plane" mode is the classical multiwire proportional chamber problem in which sense wires move alternately up or down out of their plane. In the "in plane" mode, all sense wires move in the same direction within their plane. In the sample calculation shown in Fig. 3, as g increases the stability improves in the "in plane" mode but degrades in the

"out of plane" mode. The most stable choice is at the crossing point where the two modes are equally dangerous — at $g \approx s/2$ in this example.

In light of the above, we have fixed $Q(\text{grid})/Q(\text{sense})$ to -0.4 and g/s to 2/3. The latter value is a compromise between field shaping and electrostatic stability. Then the other parameters of the jet cell are determined by the sense wire charge and spacing. The sense wire charge is set by the gas gain. Compared to gases consisting mostly of argon, DME requires almost twice the charge density (≈ 0.72 esu/cm on a 25 μm dia sense wire) to achieve a reasonable electron multiplication ($\approx 5 \times 10^4$). In DME the transverse diffusion over a fixed drift distance reaches a broad minimum [1] near an electric field of ≈ 1.9 kV/cm. Choosing that field strength for the uniform-field region fixes the sense-wire spacing at ≈ 4.6 mm (0.18 inches). Fortunately this is a practical value. Enough primary ionization is produced in 4.6 mm of DME at atmospheric pressure. Also this is close to the smallest spacing that we have been able to achieve using feed-throughs for each wire mounted on a thin bulkhead, a construction method that minimizes radiation thickness at the chamber ends. The maximum distance along the drift direction (16 mm) is set by the need to collect all ionization electrons well within the 3.5 μsec interval between Fermilab beam crossings.

Clearly, the fact that these optimizations result in a practical sense wire spacing is fortuitous. Different circumstances might require an extra degree of freedom, for example an adjustable charge density on a third grid added in the median plane. Nevertheless the optima are broad enough that other gases likely can be used with this design. For example, in a gas consisting mainly of CO_2 operated at a uniform field of 1 kV/cm and the same sense wire charge, $Q(\text{grid})/Q(\text{sense})$ becomes -0.68 for the same sense wire spacing, still a reasonable value in light of Fig. 2a.

Figure 4 shows a partial cross-section of the vertex chamber as finally designed. It will occupy the region from 3 to 17 cm in radius. The chamber is being constructed in three layers that are mechanically independent, with the wires in each layer supported only by

the carbon-fiber tube at its inside radius. The segmented construction permits the use of up to six layers of cathode pads to supplement charge division in providing longitudinal information. The reliability of the chamber is also enhanced. A fraction of it can be removed for repair, or permanently if other needs for space arise. The inner layer consists of 16 jet cells and the outer layers of 32 cells each.

Figure 5 exhibits a single vertex chamber cell from the inner layer (the relevant wires are indicated by solid points). Allowing for sharing of wires between cells, one cell includes 8 sense, 18 grid, 16 cathode, and 16 "fine field cage" wires. The sense wires are 25-μm NiCoTin stretched at 75 g, and others are 152-μm gold-plated Al stretched at 350 g. Electric fields at the surfaces of negatively charged wires are less than $\approx$ 20 kV/cm. The "fine field cage" wires at the inner and outer radius maintain the field uniformity away from the center of the cell. Serving the same purpose are a similar number of "coarse field cage" strip electrodes (not shown in Fig. 5) mounted on the nearby cylindrical surfaces. To resolve ambiguities in drift direction, alternate sense wires are staggered by $\pm$ 100 μm, and cells in the three layers are also staggered. Voltages on each wire were optimized using a realistic electrostatic simulation of this cell, including edge effects.

III. One-Cell Model

The chamber tested was constructed as a full-length model of a single cell of the inner layer of the detector. The model differed from the final design in two ways: sense wires in the model cell were not staggered; and mechanical support structures and wire terminations were different from the final design. In particular, at one end of the chamber each sense wire had an additional 100 pF of cable capacitance to ground; at both ends, the sense wires were connected to preamps through small (200 pF) blocking capacitors. By building a model chamber with a simplified mechanical structure we were able to test the basic performance characteristics of the planned chamber before completing the detailed mechanical design. These differences aside, the test chamber is an accurate electrostatic

model of the fundamental cell in the final detector's inner layer. Except for the sense wire staggering, its geometry is also shown in Fig. 5. In addition to the wires comprising one cell, the test chamber also included two planes of wires (open circles) outside the cell to simulate the effect of neighboring cells.

IV. Beam Test

The model chamber was tested in a $0.8 - 10$ GeV/c secondary beam at the Brookhaven Alternating-Gradient Synchrotron intermittently over a period of about four weeks. Other drift chambers and scintillators were located upstream as part of a general test of the D-Zero tracking system. These were useful for ensuring that a charged beam particle had passed through the chamber. However, the beam divergence and multiple Coulomb scattering were such that the upstream information could not be used directly to determine the distance vs. time relation or the single-hit accuracy of the chamber under test.

For the whole test the model chamber was filled with DME at atmospheric pressure. The DME used was specified to contain ≤ 1 ppm of Freon-11 impurity, and was measured by the vendor [6] to meet this specification. It was delivered to the chamber directly from the bottle, with no additional purification. The chamber was operated at $Q(\text{sense}) = 0.75$ esu/cm and (for circumstantial reasons) a uniform drift field of 2.3 rather than 1.9 kV/cm. This shifted $Q(\text{grid})/Q(\text{sense})$ from -0.4 to -0.27. Signals at either end of the sense wires were preamplified by circuits based on the Fujitsu MB43458 four-channel chip. After ≈ 15 m of 1.4 mm diameter coaxial cable they were shaped and further amplified. After another ≈ 50 m of 2.5 mm cable, the signals were fed to a flash ADC (FADC) based on the Sony CX20116 8-bit 100-MHz chip. Although the shaper amplifiers were capable of shortening and symmetrizing these pulses, for this test they were used only to amplify and to compensate for the cable attenuation at high frequencies. Because of timing difficulties peculiar to this test layout, the FADC's were not sensitive to early chamber pulses corresponding to hits within about 1 mm of the sense wires.

In general, the model chamber performed extremely well. No high voltage trips occurred and no evidence for wire instability was observed. The combined current on the eight sense wires ranged up to about 10 μA during beam bursts, but stayed consistently below 10 nA in the short intervals between them. At the preamp input the typical charge per pulse was about 1 pC, corresponding to an estimated gas gain of $\approx 8 \times 10^4$. The drift velocity in the uniform-field region was determined by comparing maximum observed drift times for wires with different maximum drift distances. It was found to be 8.3 μm/nsec, in agreement with previous measurements [2] referenced to the calculated electric field. From the dependence of mean pulse area on drift distance for a single wire, a mean free path for electron attachment of 3.9 cm was measured. For operation in the experiment, it will be necessary to improve the gas purity in order to realize a mean free path > 10 cm, large compared to the 1.6 cm maximum drift distance.

V. Position Accuracy Measurements

Analysis of the flash digitized chamber output requires two steps: recognition of a pulse (hit finding) and calculation of the drift time of the pulse. The hit-finding algorithm used was based primarily on differences between counts in successive FADC buckets. A pulse was defined as a group of consecutive buckets with recognizable leading and trailing edges. A leading edge was defined as a set of at least two successive differences ≥ 7 FADC counts. A trailing edge was required to have two successive differences between $+2$ and -10 FADC counts, with the last two buckets each having ≤ 15 FADC counts (after pedestal subtraction). Eventually a similar algorithm will be implemented in the FADC hardware. The combined efficiency of the test chamber and of this hit finder was measured to be $\geq 99\%$ per hit.

The algorithm for determining the drift time of a pulse was designed to be sensitive to the time of the pulse's leading edge. In a low diffusion gas like DME, the arrival time of the first electron (or cluster of electrons) is expected to be a more accurate measure of

track position than is the center of gravity of the pulse. Like the hit-finding algorithm, the pulse time algorithm was based on differences between successive FADC buckets [7]. The drift time was assigned by calculating a weighted average of these differences, using only the positive-going part of the pulse. The first bucket was assigned a unit weight, and the weight of each succeeding bucket was reduced by half. By averaging only over the leading edge of the pulse, and assigning greater weights to earlier buckets, this algorithm is more sensitive to the arrival time of the first cluster of electrons, and less sensitive to pulse broadening due to differences in drift time for electrons originating at different points along the track.

The relative position measurement accuracy of the chamber was measured by examining sets of three consecutive wires, each with a single isolated hit present (referred to as 'hit triplets'). The position of the center hit of the triplet is compared to the average of the outer pair of hits. The rms of this residual is greater than the rms of the error on a single hit by a factor $\sqrt{3/2}$. The rms error on a single hit is shown as a function of drift distance in Fig. 6. The triplets used were required to lie at least 2 mm from the sense wire plane; the right-hand border of the plot corresponds to the maximum drift distance. The measured accuracy varies from $\approx 30\mu$m for drift distances of $2-4$ mm, to $\approx 70\mu$m for drift distances of $9-11$ mm. The average accuracy over the range $2-11$ mm is $\approx 50\mu$m.

The single-hit accuracy plotted in Fig. 6 deserves two comments. The first is that comparisons of hit times for neighboring wires give the relative rather than the absolute accuracy of the chamber measurement. Systematic effects such as wire misplacement and deviations from the nominal drift distance vs. drift time relationship would not be reflected in these results. A great deal of calibration effort with the final chamber will be necessary to avoid degrading this intrinsic accuracy.

The second observation is that the single-hit accuracy worsens with drift distance at a rate considerably faster than would be expected from the effects of diffusion in DME. We have performed several tests to investigate this effect. The data contributing to Fig. 6 were

taken with the beam particles making an angle of about 0.1 rad with respect to the sense plane. Thus the effects of any crosstalk between neighboring wires would not be expected to produce anomalously small residuals. We have compared data taken at instantaneous rates corresponding to low ($\approx 0.5 \times 10^{29}$) and high ($\approx 10^{30}\text{cm}^{-2}\text{sec}^{-1}$) luminosity at the Fermilab collider. Under high luminosity conditions the single-hit accuracy degraded only by $\sim 10\%$, ruling out space charge as a dominant factor. A remaining explanation is the reduction in pulse height due to electron attachment in the DME, combined with possible slewing and increased effects of noise in the determination of its leading edge. This will be a focus of study in tests of the final chamber.

VI. Pulse-Pair Resolution

The recorded FADC information made it easy to study the chamber's pulse-pair resolution capabilities. To measure the efficiency for detecting a second pulse, we randomly superimposed pulses from different events and applied the same hit finder to the combined data. Overlapping pulses were recognized by appearance of two successive leading edges, with no trailing edge criterion satisfied by the intervening data. No special cuts were applied to the hits used in this study, except that both the original and the added hits themselves were required to be isolated.

Figure 7 shows the efficiency for finding the second hit as a function of the separation of the two hits. For pulse separations greater than 84 nsec, or 0.7 mm, the efficiency exceeds 90%. We also compared the drift times measured for the superimposed pulses with the expected times determined from the original isolated pulses. The earlier pulse time was found to be insensitive to the presence of the later pulse, while for pulses with fixed separation ≥ 0.7 mm a mean shift of ≤ 3 nsec was observed in the measured time of the later pulse. More important is the spread in measured times induced by the overlapping pulse. For the later hit this spread is < 6 nsec rms for hit separations ≥ 0.7 mm. Thus, for hit separations of ≥ 0.7 mm, the smearing of the hit position due to the presence of

the earlier pulse is $< 50\mu$m. For hits with ≥ 1 mm separation, the smearing is less than 35 μm.

VII. Other Results

We have made preliminary measurements of the accuracy of axial coordinate determination by charge division with this model. The cabling asymmetry in the model chamber and the not yet optimized pulse shaping degraded its performance, compared with the final chamber, but the test results can still set limits on the expected accuracy. A resolution of 0.8 - 1.6 cm (rms) in the axial coordinate was measured, with an average value of 1.33 cm. The linearity of the charge division response is better than 0.2% rms. This measured performance indicates that the final chamber can achieve an axial coordinate resolution that is better than 1% of the wire length, or ≈ 1 cm.

We have also measured the dE/dx resolution of the model. While the vertex chamber is not intended to provide a precise measure of ionization energy loss, it is desirable to use dE/dx information to distinguish between overlapped e^+e^- pairs (from γ conversions) and single electrons. The measured response to single tracks can be used to estimate crudely the response to a pair of overlapped tracks. Ignoring effects of gain saturation and wire-to-wire correlations, we estimate that overlapped tracks can be rejected more than 99% of the time in each of the three detector layers, while retaining an efficiency for single (isolated) track segments $> 98\%$ in each layer.

VIII. Summary

We have tested a one-cell model of the vertex detector being constructed for the D-Zero experiment at the Fermilab collider. The full-length model cell accurately simulates the electrostatics of the planned chamber. Position measurement accuracy of 30 - 80 μm is obtained for drift distances between 2 and 11 mm. Pulse-pair resolution of 0.7 mm is achieved for 90% of all pulses. Although work continues on understanding the contributions

of systematic errors to the test data, the performance achieved already meets the basic requirements for use in D-Zero. Both the position accuracy and the two track resolution are significantly better than would be expected from the use of saturated gas in a similar chamber. We conclude that both the basic design of this chamber and its use of DME are viable for the application envisaged.

Acknowledgements

We are indebted to our colleagues who participated in the D-Zero beam test at Brookhaven, especially M. Rijssenbeek, M. L. Good, and J. D. Turk, and to the AGS staff who made it possible. We thank T. Weber for skillful help in chamber construction. This research was supported in part by the U. S. Department of Energy through Contract No. DE-AC03-76SF00098.

References

[1] F. Villa, Nucl. Instrum. and Methods 217, 273 (1983).

[2] G. Bari et al., Nucl. Instrum. and Methods A251, 292 (1986); M. Basile et al., Nucl. Instrum. and Methods A239, 497 (1985).

[3] W. B. Atwood et al., Nucl. Instrum. and Methods A252, 295 (1986).

[4] J. Alexander et al., Nucl. Instrum. and Methods A252, 350 (1986).

[5] I. Juricic and J. A. Kadyk, in Proceedings of the Workshop on Radiation Damage to Wire Chambers, LBL report LBL-21170 (1986).

[6] Matheson Co., East Rutherford, N. J. 07073.

[7] D. Schaile, O. Schaile and J. Schwarz, Nucl. Instrum. and Methods A242, 247 (1986), use a similar approach.

Figure Captions

FIG. 1: The central tracking system for the D-Zero detector. The innermost system is the three-layer vertex detector. Next is a transition radiation detector, followed by an outer drift chamber.

FIG. 2: Calculated time interval to collect 90% of the ionization electrons produced in an infinite rectangular double-grid-plane jet cell (inset) by a charged particle moving along the direction of the arrow. The time unit is (sense wire spacing)/(drift velocity in the constant-field region). The abscissa is the ratio of total charge on both grid planes to charge on the sense plane. The parameter is the ratio of the gap between the grid planes to the sense wire spacing (= 1 in the inset). Only geometrical (not stochastic) effects are included. for the following gas types: (a) constant mobility, (b) constant drift velocity, (c) argon/4% CH_4/3% CO_2, (d) argon/10% CH_4. For (c) and (d) the constant drift field is 600 V/cm-atm.

FIG. 3: Example of calculated effective spring constant $k = d^2U/2dx^2$ for sense wire electrostatic instability in the jet cell geometry of Fig. 2, for two modes. For the "out of plane" mode, x is the coherent displacement of each sense wire alternately above and below the median plane. For the "in plane" mode, x is the coherent displacement of each sense wire within the median plane. Here U is the field energy per unit sense wire length when the sense wire spacing is 1 cm, the sense wire charge is 1 esu/cm, and the total charge on both grid planes is -43% of that on the sense plane. The abscissa is the parameter in Fig. 2. For this calculation the grid wires are taken to be fixed in position.

FIG. 4: Geometry of the vertex detector. Layer 1 has 16 cells and layers 2 and 3 have 32 cells. staggered by 1/4 cell.

FIG. 5: Vertex detector cell geometry. A single cell from layer 1, including eight sense wires (anodes) and two sets of grid wires, is shown. Cathode and field cage wires define the cell boundary. In addition to the single drift cell (solid circles), two additional

planes of wires (open circles) simulate the effect of neighboring cells in the one-cell model chamber.

FIG. 6: Position measurement accuracy, determined from local residuals of hit triplets, plotted vs. distance from the hit to the anode. Data from all eight sense wires are compatible and were summed in this plot. Hits within 2 mm of the anode are excluded.

FIG. 7: Efficiency for finding overlapping pulses. The efficiency for finding the second pulse of an overlapping pair is shown as a function of the separation between the two pulses. The efficiency exceeds 90% for pulses separated by more than 84 nsec, corresponding to 0.7 mm.

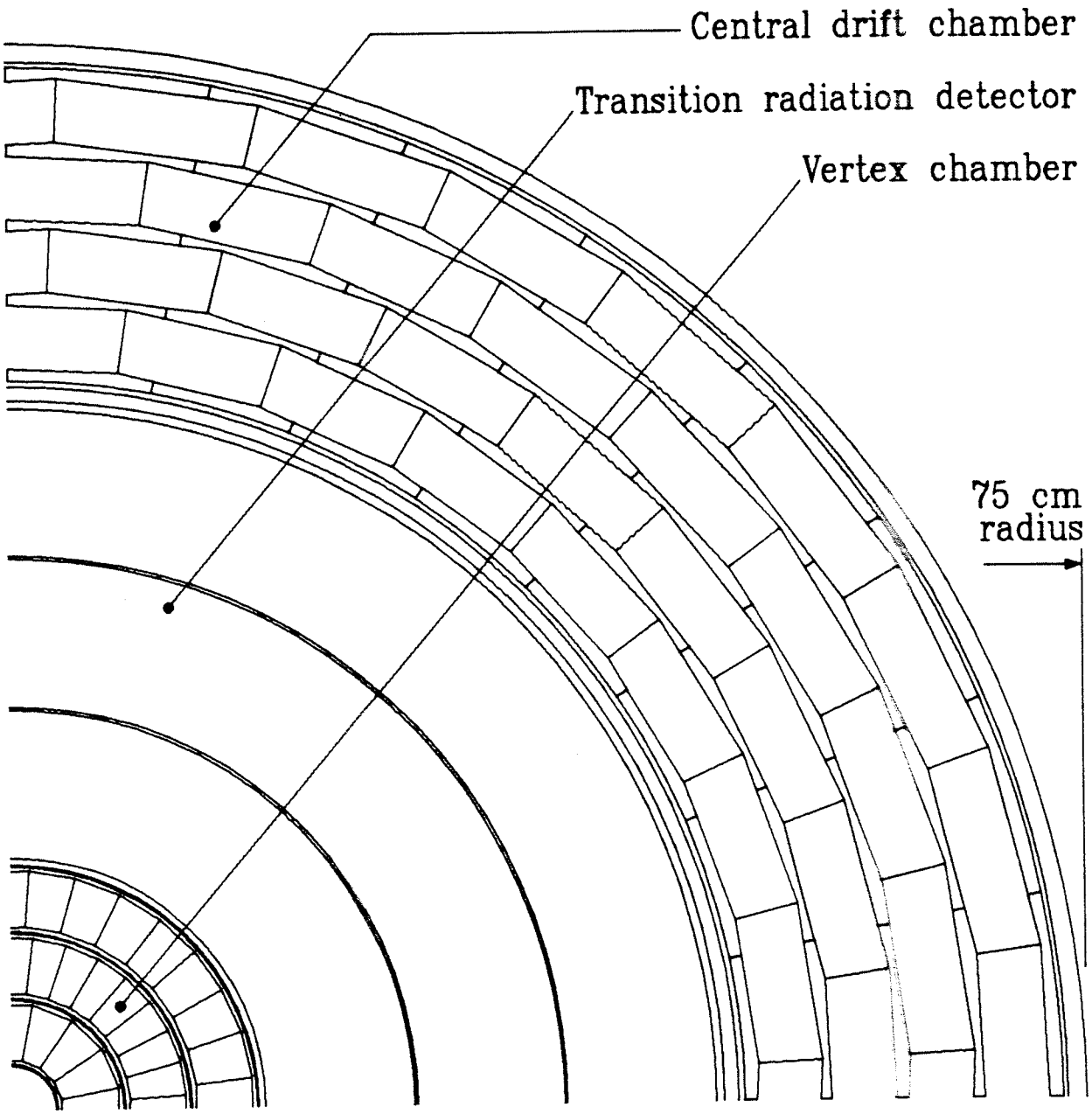
Central drift chamber
Transition radiation detector
Vertex chamber
75 cm
radius

FIG. 1

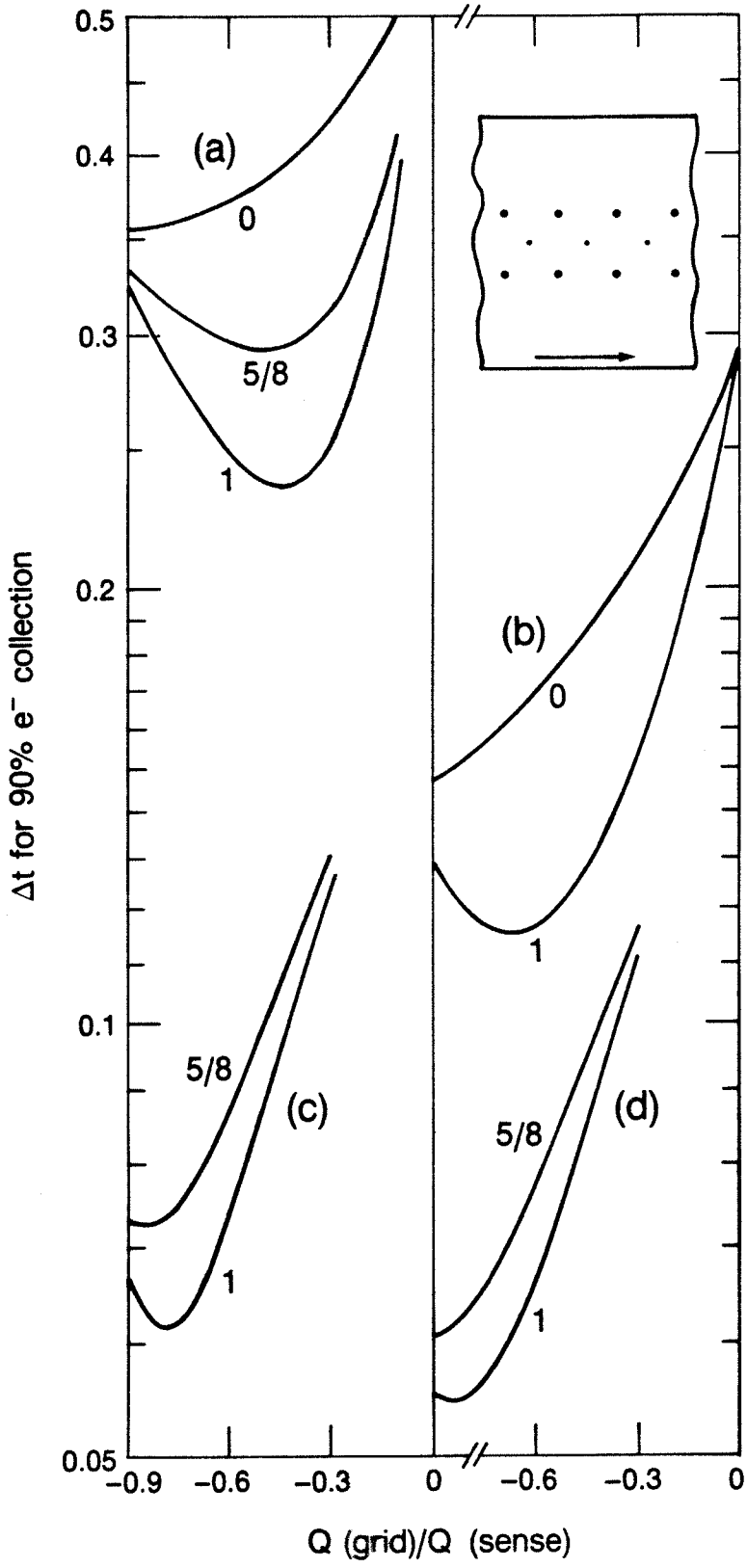

XBL 875-9660

FIG. 2

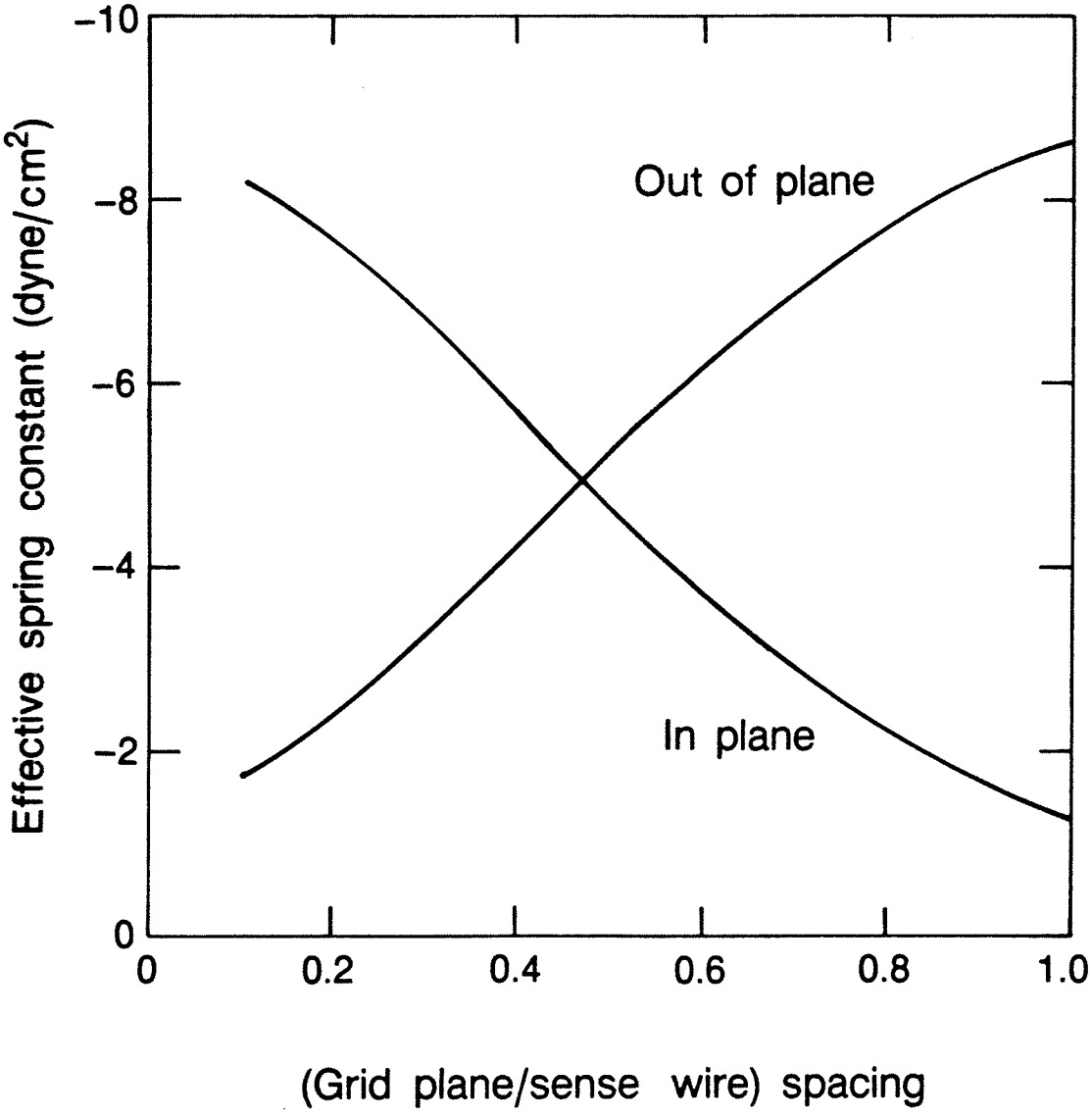

XBL 875-9661

FIG. 3

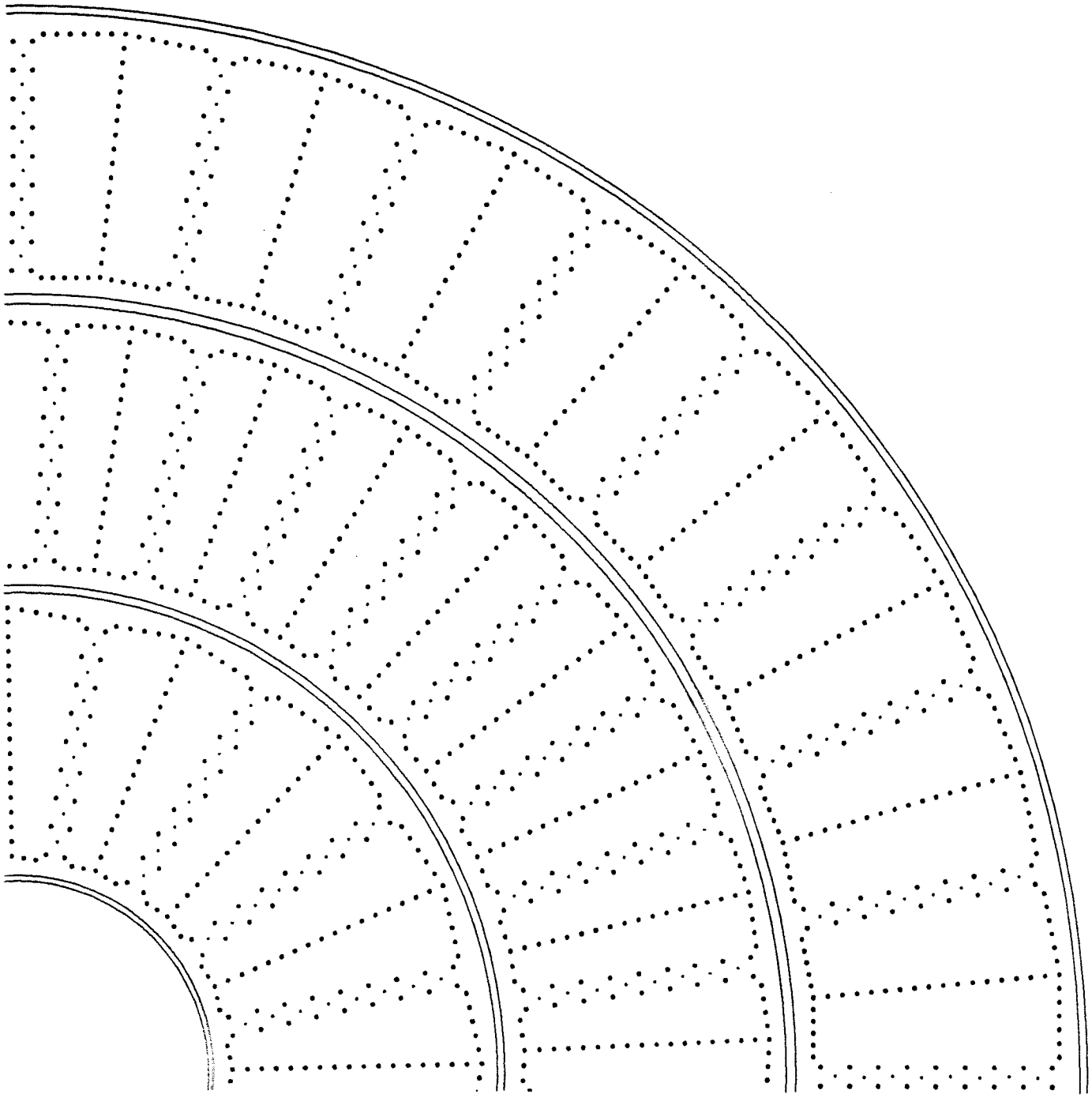

FIG. 4

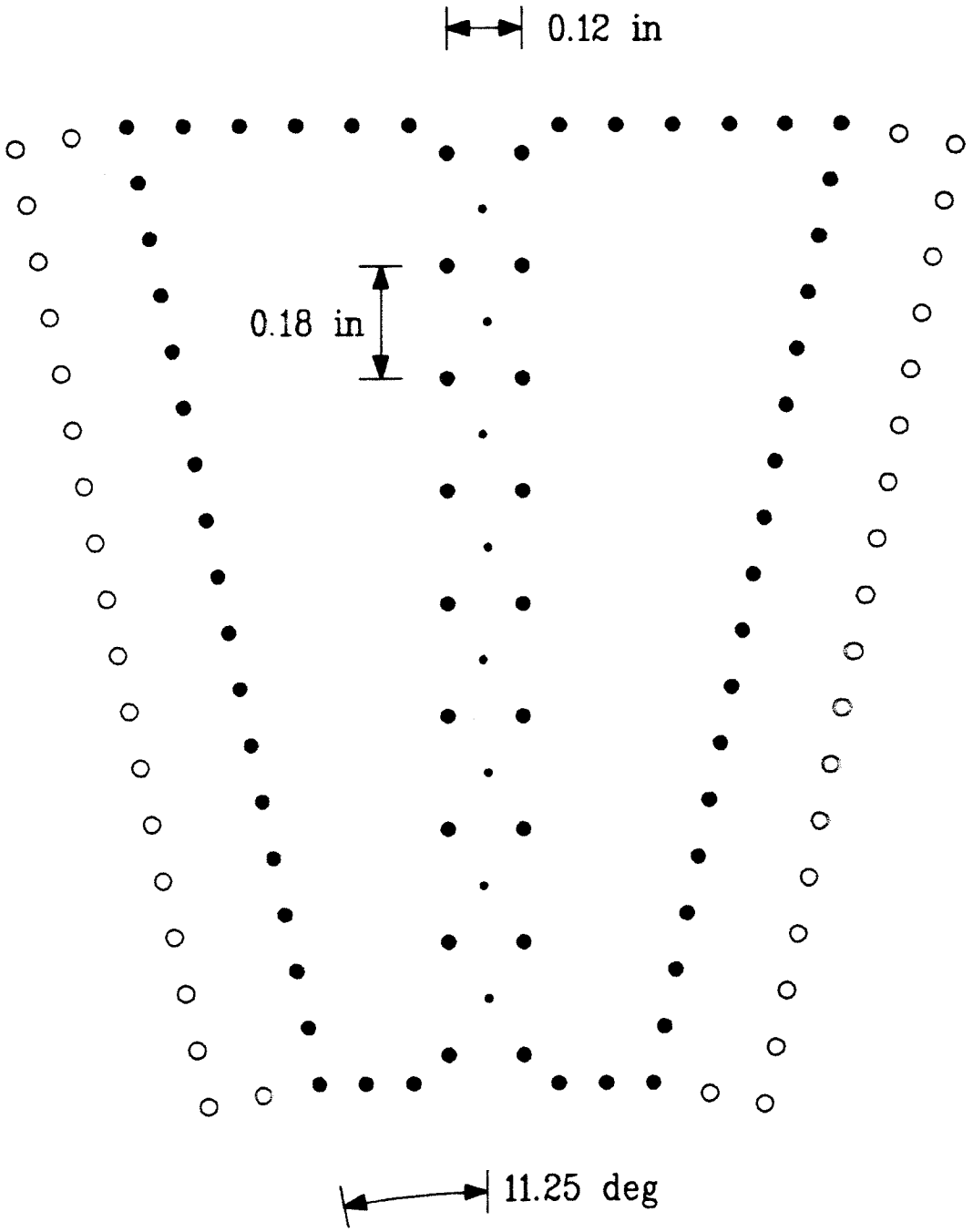

FIG. 5

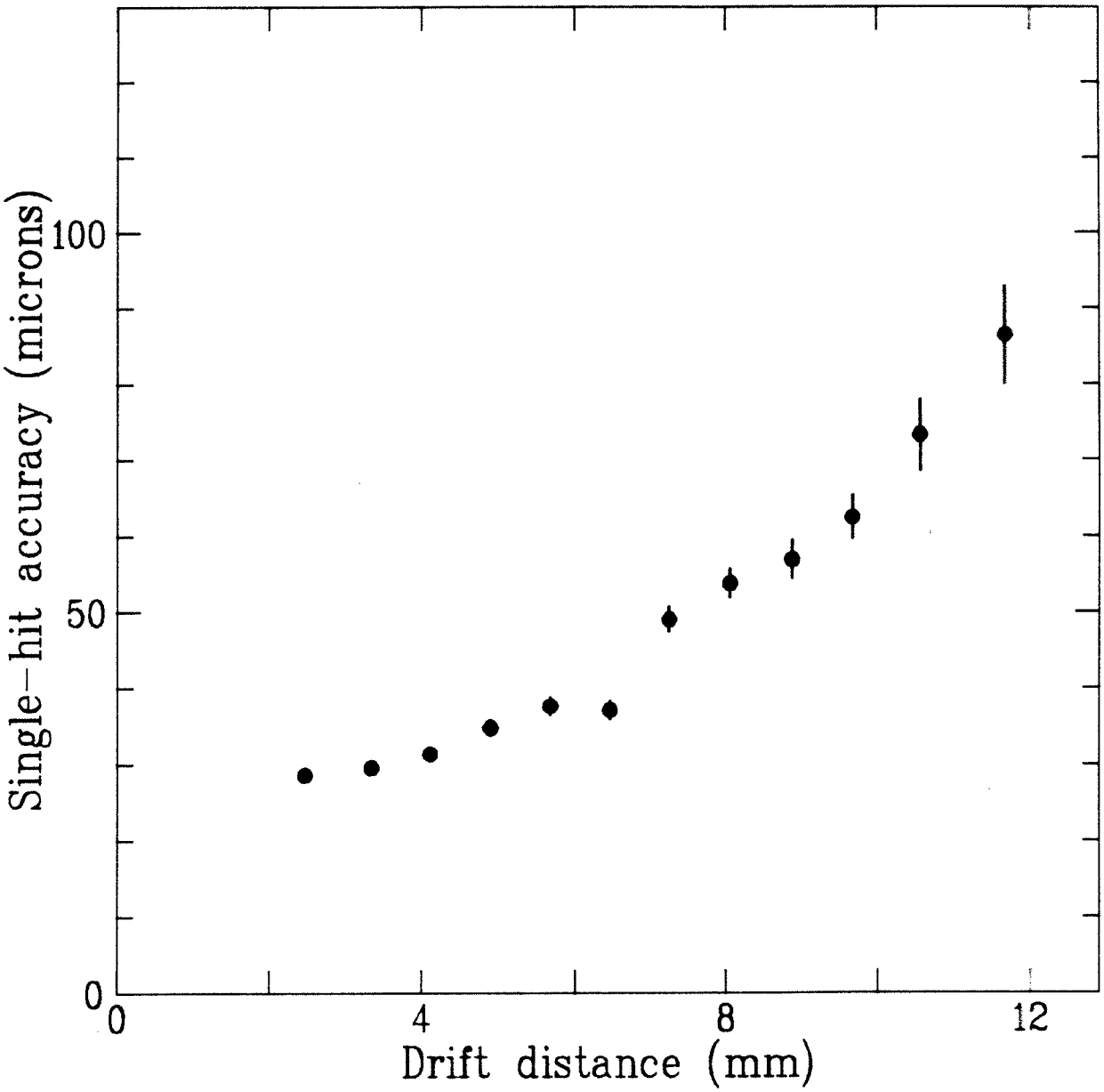
Single-hit accuracy (microns)
100
50
0
0
4
8
12
Drift distance (mm)

FIG. 6

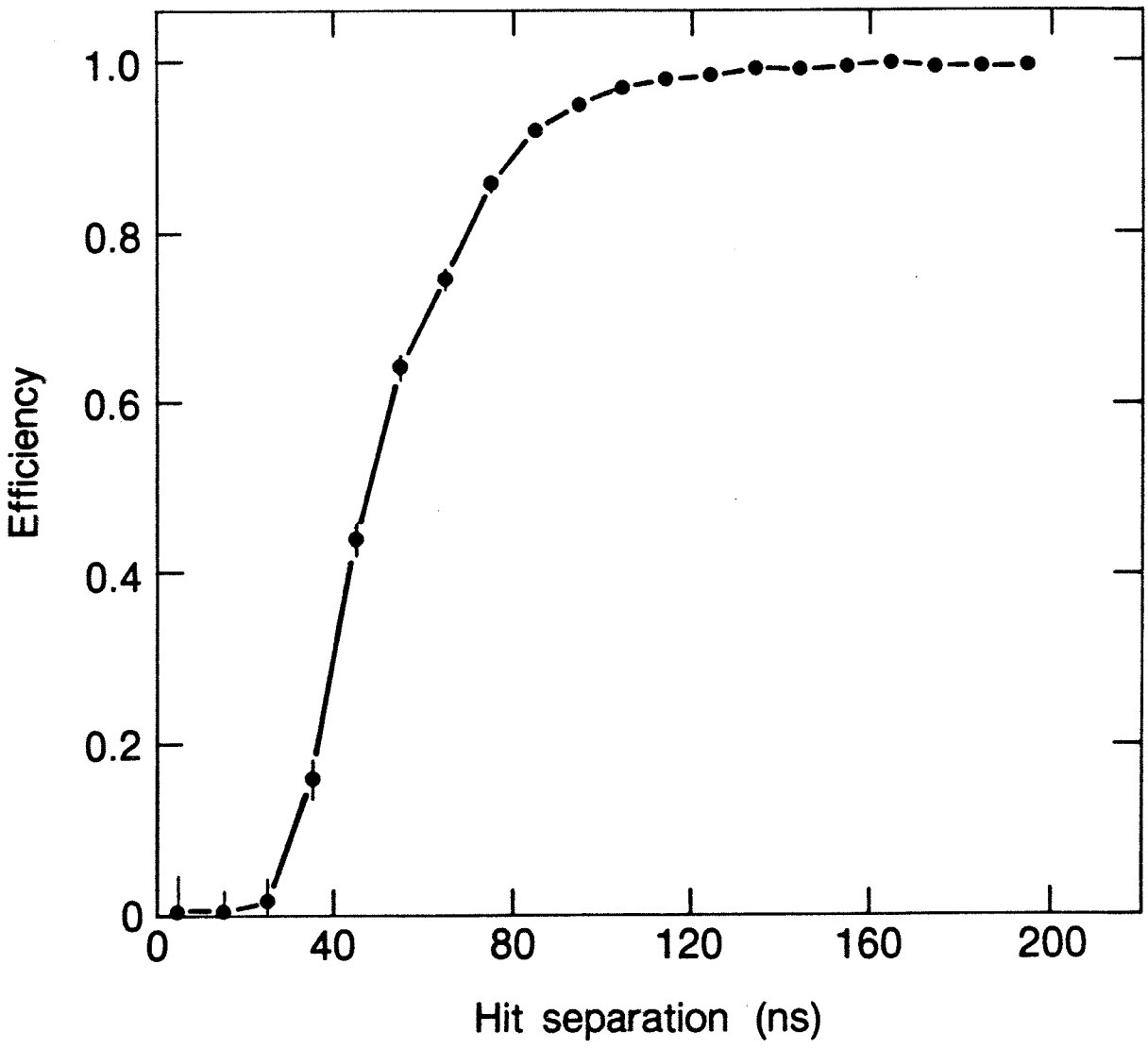

XBL 875-9662

FIG. 7